DALTON
FULL PAPER

# Co-ordination chemistry of the $[Re(NO)_2(PR_3)_2]^+$ fragment: crystallographic and computational studies †

**Heiko Jacobsen, Katja Heinze, Angela Llamazares, Helmut W. Schmalle, Georg Artus and Heinz Berke**

*Anorganisch-chemisches Institut, Universität Zürich, Winterthurerstr. 190, CH-8057 Zürich, Switzerland*

***Received 19th February 1999, Accepted 8th April 1999***

The cationic complexes $[Re(NO)_2(PCy_3)_2]^+$ **I**$^+$ and $[Re(NO)_2(PR_3)_2L]^+$ [L = CO, R = Cy **III**$^+$; L = $C_6H_5CHO$, R = Cy **IV**$^+$; L = $ONRe(NO)(PR_3)_2H$, R = $^i$Pr **V**$^+$] have been synthesized and their structures determined. The counter ion in all cases is $[B\{3,5\text{-}(F_3C)_2C_6H_3\}_4]^-$. Complex **I**$^+$ adopts the $C_{2v}$ butterfly geometry, whereas **III**$^+$ takes on a trigonal bipyramidal (TBP) co-ordination. In **IV**$^+$ and **V**$^+$ one of the nitrosyl ligands is strongly bent, and a shape analysis suggests that the co-ordination geometry of the $[Re(NO)_2(PR_3)_2L]^+$ core is best described as tetragonal pyramidal (TP). A computational study based on density functional theory showed how steric effects due to the ligand L induce the NO bend, and subsequently lead to the change in co-ordination from TBP to TP. Examination of a series of model compounds $[Re(NO)_2(PH_3)_2L]^+$ showed further how the π donor and acceptor properties of the ligand L are reflected in the P–Re–P and N–Re–N angles of the complexes.

The nitrosyl ligand[1] plays a special role in transition metal chemistry. It is capable of supporting different oxidation states of the metal center *via* different co-ordination modes, and has the capability to activate metal–ligand bonds. Prominent examples of the latter are nitrosyl substituted transition metal hydride complexes,[2] in which the M–H bond shows an increased reactivity toward alkyne insertion and carbonyl reduction.

In the context of structural chemistry and reactivity exploration in this class of compounds, we have prepared a series of mononitrosyl hydrido complexes containing various phosphorus donor ligands, as well as chromium,[3] tungsten[4] and rhenium[5] centers. The increased hydridicity[2] of these compounds has been probed by the interaction with acidic substrates.[6] We also directed our efforts towards the synthesis of dinitrosyl hydride derivatives, which should possess even more activated metal–hydrogen bonds. In contrast to their carbonyl analogues $[Mn(CO)_3(PR_3)_2H]$, manganese complexes of the general formula $[Mn(NO)_2(PR_3)_2H]$ undergo facile insertions of polar unsaturated molecules.[7] We then set out to extend this chemistry to the related rhenium complexes, and provided synthetic access to compounds of the type $[Re(NO)_2(PR_3)_2H]$.[8] During the course of this work we were also able to isolate and characterize the 16 electron fragment $[Re(NO)_2(PCy_3)_2]^+$, as well as a variety of complexes of the type $[Re(NO)_2(PR_3)_2L]^+$.

The present paper is mainly concerned with structural aspects of $[Re(NO)_2(PR_3)_2L]^{n+}$ complexes ($n = 0$ or 1). In particular, we want to address the question of how structural changes in the $[Re(NO)_2(PR_3)_2]^+$ fragment under co-ordination of a ligand L might provide information about the nature of the Re–L bond. The variation in the co-ordination geometry might further influence the reactivity of the species. The experimental part is complemented by a computational study based on density functional theory (DFT).[9] The molecular and electronic structure of 12 model compounds were investigated, as displayed in Fig. 1. The calculations were implemented to support the results obtained from the X-ray crystallographic analyses, and to provide explanations for the observed structural features.

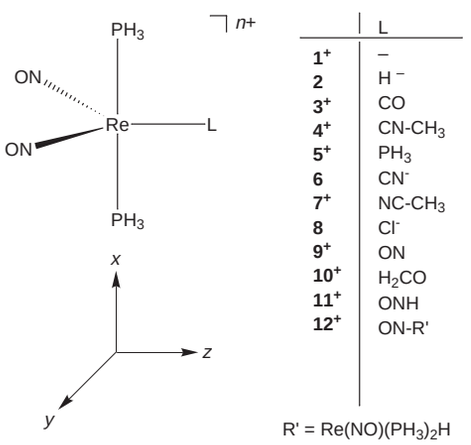


**Fig. 1** The $[Re(NO)_2(PH_3)_2L]^{n+}$ model complexes $n = 0$ or 1.

## Results and discussion

### Crystallographic studies

We determined the crystal structures of $[Re(NO)_2(PCy_3)_2][BAr^F_4]$, and of the three $[Re(NO)_2(PR_3)_2L][BAr^F_4]$ complexes with L = CO, $C_6H_5CHO$, or $ONRe(NO)(PR_3)_2H$. Here, $[BAr^F_4]$ stands for $[B\{3,5\text{-}(F_3C)_2C_6H_3\}_4]^-$. The anion is excluded from our discussion, which is focussed on the structural elements of the rhenium fragments which will be analysed together with those of $Re(NO)_2(PR_3)_2H$.[8] We shall refer to the metal fragments as $[Re(NO)_2(PCy_3)_2]^+$ **I**$^+$, $Re(NO)_2(P^iPr_3)_2H$ **II**, $[Re(NO)_2(PCy_3)_2(CO)]^+$ **III**$^+$, $[Re(NO)_2(PCy_3)_2(C_6H_5CHO)]^+$ **IV**$^+$, and $[Re(NO)_2(P^iPr_3)_2\{ONRe(NO)(P^iPr_3)_2H\}]^+$ **V**$^+$. Selected structural parameters for these complexes are presented in Table 1. For in-depth background information a reader should refer to the deposited crystallographic data.

**$[Re(NO)_2(PCy_3)_2]^+$ I$^+$.** A view of the molecular structure of complex **I**$^+$ in the crystal is displayed in Fig. 2. It can be

† *Supplementary data available*: optimized geometries and eigenvalues. For direct electronic access see http://www.rsc.org/suppdata/dt/1999/1717/, otherwise available from BLDSC (No. SUP 57540, 4 pp.) or the RSC Library. See Instructions for Authors, 1999, Issue 1 (http://www.rsc.org/dalton).

**Table 1** Selected bond lengths and angles[a] for $[Re(NO)_2(PR_3)_2L]^{n+}$ complexes ($n = 0$ or 1)

| | R | L | Re–L | Re–P | Re–N | N–O | P–Re–P | Re–N–O | N–Re–N | Other | |
|---|---|---|---|---|---|---|---|---|---|---|---|
| **I**$^+$ | Cy | — | — | 245.4(3) | 173.5(10) | 122.5(12) | 159.93(8) | 166.9(9) | 115.9(4) | | |
| | | | | 246.2(3) | 176.6(8) | 118.0(11) | | 165.7(9) | | | |
| **II** | $^i$Pr | $H^-$ | 177.93(2) | 242.8(2) | 180.4(7) | 119.3(9) | 153.89(6) | 173.1(8) | 127.4(3) | L–Re–N | 122.3(3) |
| | | | | 242.1(2) | 178.0(7) | 122.7(9) | | 175.4(7) | | | 110.2(2) |
| **III**$^+$ | Cy | CO | 197.9(6) | 247.4(2) | 179.0(7) | 119.1(9) | 169.62(5) | 174.0(6) | 121.5(3) | C–O | 114.6(8) |
| | | | | 248.8(1) | 182.5(5) | 117.6(1) | | 176.3(6) | | L–Re–N | 129.6(3) |
| | | | | | | | | | | | 108.9(3) |
| **IV**$^+$ | Cy | $C_6H_5CHO$ | 218.8(3) | 248.4(1) | 175.8(4) | 119.9(5) | 158.40(4) | 150.9(3) | 108.8(2) | C–O | 123.6(5) |
| | | | | 248.8(1) | 181.1(4) | 120.4(5) | | 175.9(4) | | L–Re–N | 91.6(1) |
| | | | | | | | | | | | 159.5(1) |
| **V**$^+$ | $^i$Pr | ONR′[b] | 219.9(9) | 247.2(4) | 178(1) | 120(1) | 162.8(1) | 158(1) | 111.4(6) | O–N | 125(2) |
| | | | | 248.2(4) | 180(2) | 117(2) | | 172(1) | | L–Re–N | 97.4(5) |
| | | | | | | | | | | | 150.7(5) |

[a] Distances in pm, angles in (°). [b] R′ = $Re(NO)(P^iPr_3)_2H$.

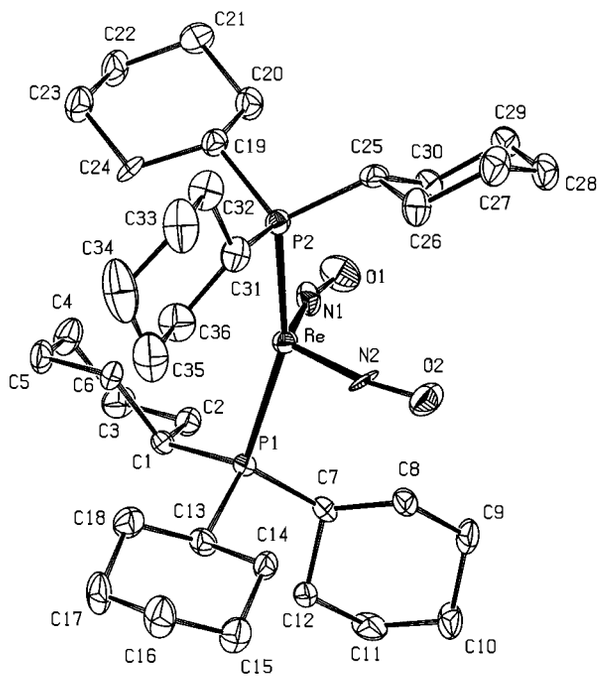


**Fig. 2** Molecular structure of complex **I**$^+$. Displacement ellipsoids are shown at the 30% level. Hydrogen atoms are omitted for clarity. Not shown are the counter ion and solvate molecules.

obtained almost quantitatively by the reaction of **II** with $[(C_6H_5)_3C][BAr^F_4]$ in benzene. The complex can be described as a distorted $C_{2v}$ butterfly fragment, which is obtained on removing one equatorial ligand from an ideal trigonal bipyramidal arrangement. Important geometric features are a P–Re–P angle some 20° smaller than the ideal value of 180°, and an N–Re–N angle close to 120°. The phosphorus atoms are bent away from the NO groups; the nitrosyl ligands themselves are not linearly co-ordinated but show a cisoid bend of about 15°.

Structures of a variety of $[M(NO)_2(PR_3)_2]^{n+}$ compounds ($n = 0$ or 1; M = Fe, Ru, Os, Co, Rh or Ir), are described in the literature.[10] All these complexes having electron counts of 18 (or 17),[10m] exhibit the co-ordination geometry of a distorted tetrahedron,‡ and therefore cannot be compared with **I**$^+$. However, the crystal structures of two isoelectronic carbonyl compounds are known, namely $[Rh(CO)_2\{P(2,4,6\text{-}(MeO)_3C_6H_2)_3\}_2]^+$ and $[Ru(CO)_2(P'Bu_2Me)_2]$.[12,13] The latter complex[13] possesses the same $C_{2v}$ butterfly geometry as that of **I**$^+$, whereas the former[12] shows square planar co-ordination. Thus, it was not initially clear which geometry the fragment **I**$^+$ might adopt.

‡ For an orbital analysis of $MX_2(NO)_2$ systems by extended Hückel theory compare ref. 10(*m*). See also ref. 11.

The main aspects of the Walsh diagram for the planar $D_{4h}$ into bent $C_{2v}$ transformation are established for $ML_4$ complexes,[14a] and Caulton and co-workers[13] have adapted this analysis for compounds of the type $M(CO)_2(PR_3)_2$. The $d_{z^2}$ orbital is stabilized under bending, because of diminished overlap with the $\sigma_{CO}$ lone pair, and because back bonding into $\pi^*_{CO}$ is now possible.[15] The $d_{xz}$ orbital is also stabilized by back donation in the bent geometry. On the other hand, the $d_{yz}$ orbital is strongly destabilized in the bent structure, due to diminished overlap with $\pi^*_{CO}$, and due to antibonding overlap with the $\sigma_{CO}$ lone pair. The important interactions are shown below [adopted from ref. 13(*a*)] (see also Fig. 7).

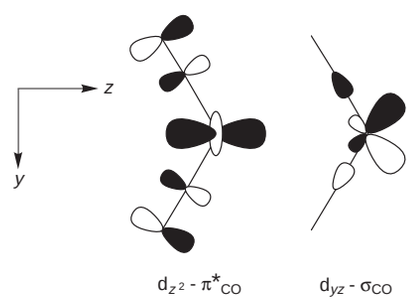


The antibonding interaction between $d_{yz}$ and $\sigma_{CO}$ or $\sigma_{NO}$, respectively, can be reduced by a cisoid bend of the M–C–O or the M–N–O angle. This explains the observed non-linear co-ordination of the nitrosyl ligands in complex **I**$^+$. The preferred geometry will be non-planar if the stabilization due to back donation outweighs the destabilizing interactions. The important criterion is the energetic match between the metal donor orbitals and the ligand $\pi^*_{XO}$ (X = C or N) acceptor orbitals.[13] In **I**$^+$ the electron rich metal center $Re^{-I}$ possesses d orbitals which are at relatively high energies. These are energetically well suited for an interaction with the $\pi^*_{NO}$ orbitals. Thus, **I**$^+$ prefers the $C_{2v}$ butterfly geometry. The same holds for the neutral ruthenium complex $[Ru(CO)_2(P'Bu_2Me)_2]$.[13] In contrast, the low energy of the d orbitals of $Rh^I$ in $[Rh(CO)_2\{P(2,4,6\text{-}(MeO)_3C_6H_2)_3\}_2]^+$ decreases the role of back donation. This complex therefore adopts the square planar geometry.[12]

In a DFT calculation we have tried to optimize the square planar geometry of the model complex $[Re(NO)_2(PH_3)_2]^+$ **1**$^+$. This could only be achieved by employing angular constraints, and enforcing a planar co-ordination environment, which indicates that planar **1**$^+$ is not a local minimum on the potential energy surface. This hypothetical molecule should have a triplet state, since one of the rhenium d-based orbitals and one combination of NO π* orbitals are accidentally degenerate.

**$[Re(NO)_2(P^iPr_3)_2H]$ II.** The preparation and the structure of complex **II**, as shown in Fig. 3, have already been discussed,[8]

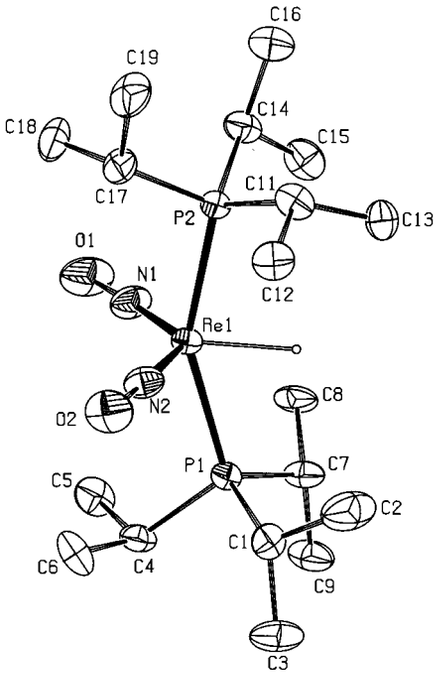


**Fig. 3** Molecular structure of complex **II**. Displacement ellipsoids are shown at the 40% level. Hydrogen atoms are omitted for clarity, except for the hydride ligand, which is displayed as a sphere with arbitrary size.

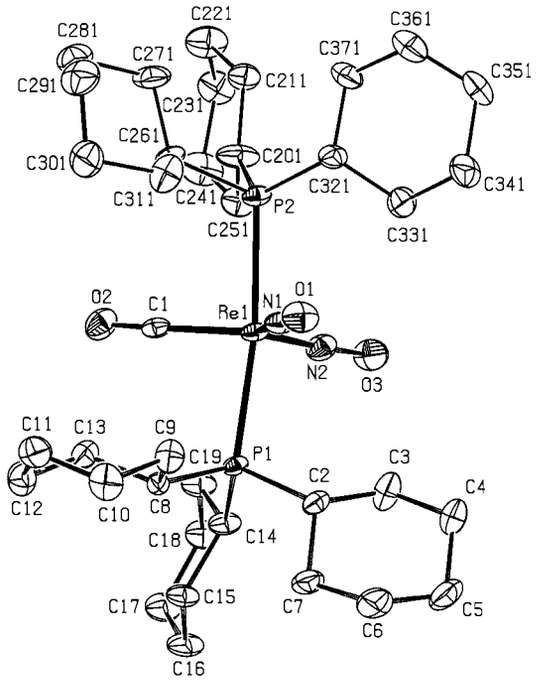


**Fig. 4** Molecular structure of complex $\mathbf{III}^+$. Details as in Fig. 2.

and we will only briefly comment on its geometry. The structure is that of a distorted trigonal bipyramidal (TBP). Compared to $\mathbf{I}^+$, we observe that the N–Re–N angle opens up by about 11° under co-ordination of the hydride ligand. At the same time, P–Re–P becomes narrower by 6°. The bending distortion of the phosphorus donor ligands is well understood.[14] Bending of the $PR_3$ groups of $[Re(NO)_2(PR_3)_2L]^{n+}$ towards the ligand site polarizes the $d_{xz}$ orbital of the metal in the direction of the π accepting nitrosyl ligands, providing better $d_{xz}$–$\pi^*_{NO}$ overlap, and enhancing the amount of back donation to NO. The degree of back bending of the $PR_3$ is limited by steric repulsion between $PR_3$ and L, and between the phosphorus ligands themselves. The small hydride ligand does not provide much steric hindrance for the bulky $P^iPr_3$ group, but it does increase the electron density on the rhenium center. Back bonding to the nitrosyl ligands becomes stronger, and as a consequence the P–Re–P angle decreases.

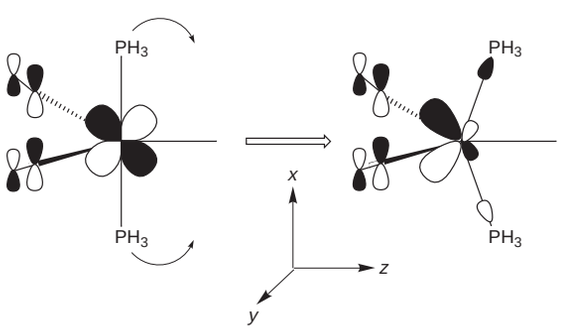


**$[Re(NO)_2(PCy_3)_2(CO)]^+$ $\mathbf{III}^+$.** Reaction of complex $\mathbf{I}^+$ with the prototypical π acceptor ligand CO leads to formation of $\mathbf{III}^+$. Its molecular geometry in the crystal is displayed in Fig. 4. One of the $PCy_3$ ligands is highly disordered, but was resolved in the course of the structure refinement. The N–Re–N angle is still larger than that in the free fragment $\mathbf{I}^+$, but the P–Re–P angle opens up by 10° (see Table 1). Since CO is competing with the NO ligands for back donation, a strong polarization of $d_{xz}$ away from the L site is no longer favorable, and consequently P–Re–P opens up. The fact that CO is competing for electron density manifests itself also in a small N–O bond contraction

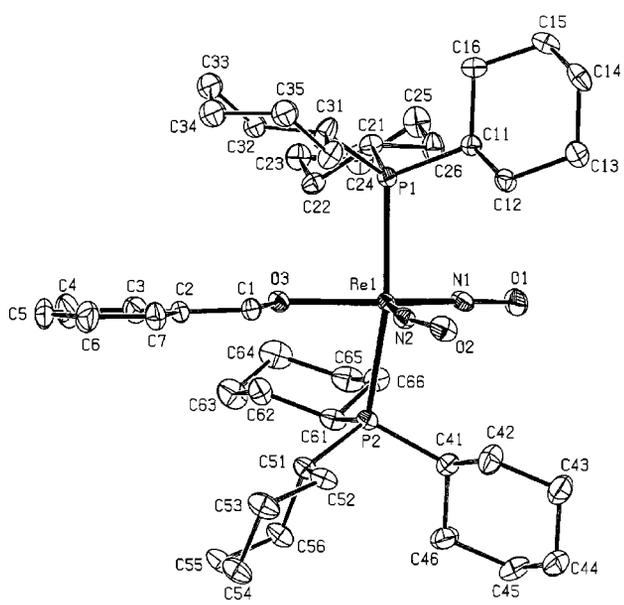


**Fig. 5** Molecular structure of complex $\mathbf{IV}^+$. Details as in Fig. 2.

[compare $d$(N–O) in $\mathbf{I}^+$ and $\mathbf{III}^+$], and a small C–O bond elongation [compare to $d$(C–O) = 112.8 pm in the gas phase[16]].

**$[Re(NO)_2(PCy_3)_2(C_6H_5CHO)]^+$ $\mathbf{IV}^+$.** Compound $\mathbf{IV}^+$ is instantaneously formed when $\mathbf{I}^+$ is treated with benzaldehyde. In this complex a new structural motif is introduced. The benzaldehyde L does not bind in a symmetrical, but rather asymmetrical fashion, as can be seen in Fig. 5. The pseudo $C_2$ rotational axis is removed, and only idealized $C_s$ symmetry is retained. Characteristic bond lengths such as Re–N and Re–P are very similar in $\mathbf{III}^+$ and $\mathbf{IV}^+$, but the co-ordination geometry is very different. The N–Re–N angle is now smaller than that of the free fragment $\mathbf{I}^+$. Furthermore, one of the nitrosyl ligands (N2O2 in Fig. 5) is strongly bent forming a Re–N–O angle of 151°. This falls right between the linear co-ordination of the $3e^-$ donor $NO^+$ (M–N–O 180°) and the bent co-ordination of the $1e^-$ donor $NO^-$ (M–N–O 120°). Two very different L–Re–N angles are observed, one being close to 90° and the other being about 160°. Thus, the co-ordination geometry of $\mathbf{IV}^+$ resembles

**Table 2** Observed $\delta$ angles[a] for $[Re(NO)_2(PR_3)_2L]^+$ complexes, together with values[b] for idealized polyhedra. Also given are the standard deviations $\sigma(\Gamma)$ (see text for definition)

| Complex | $\delta(a_1)$ | $\delta(a_2)$ | $\delta(a_3)$ | $\delta(a_4)$ | $\delta(a_5)$ | $\delta(a_6)$ | $\delta(e_1)$ | $\delta(e_2)$ | $\delta(e_3)$ | $\sigma(D_{3h})$ | $\sigma(C_{4v})$ |
|---|---|---|---|---|---|---|---|---|---|---|---|
| Ideal TBP ($D_{3h}$) | 101.5 | 101.5 | 101.5 | 101.5 | 101.5 | 101.5 | 53.1 | 53.1 | 53.1 | 0.0 | 26.9 |
| **III**$^+$ | 115.5 | 111.9 | 98.3 | 115.3 | 110.9 | 99.7 | 26.6 | 52.7 | 44.0 | 12.4 | 30.4 |
| **IV**$^+$ | 124.7 | 79.1 | 127.6 | 126.1 | 77.1 | 127.7 | 68.3 | 59.0 | 5.6 | 26.1 | 7.9 |
| **V**$^+$ | 120.3 | 85.2 | 123.8 | 122.8 | 80.9 | 123.5 | 65.5 | 52.4 | 5.9 | 23.2 | 9.7 |
| Ideal TP ($C_{4v}$) | 119.8 | 75.7 | 119.8 | 119.8 | 75.7 | 119.8 | 75.7 | 75.7 | 0.0 | 26.9 | 0.0 |

[a] In °. [b] From ref. 18(b).

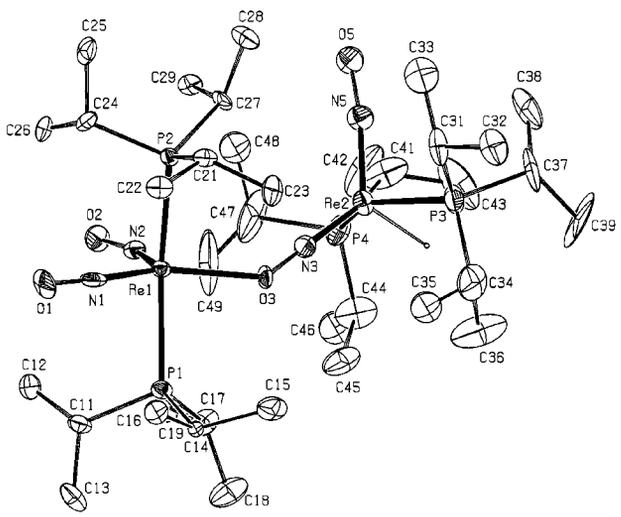


**Fig. 6** Molecular structure of complex **V**$^+$. Displacement ellipsoids are shown at the 20% level. Hydrogen atoms are omitted for clarity, except for the hydride ligand, which is displayed as a sphere with arbitrary size. Not shown is the counter ion.

more closely that of a tetragonal pyramid (TP) than that of a trigonal bipyramid (TBP). The infrared spectrum shows however, both in solution and in the solid state, a group of peaks in the carbonyl–nitrosyl region that could not be assigned (see Experimental section). We can envisage this structural change as follows:§ co-ordination of benzaldehyde L to the open co-ordination site of the $d^8$-$Re(NO)_2(PR_3)_2$ fragment induces a bend in one nitrosyl ligand. This subsequently leads to a formal oxidation of the metal center, resulting in a $d^6$-$Re(NO)_2(PR_3)_2L$ species, which is still co-ordinatively and electronically unsaturated. The preferred geometric arrangement of a $d^6$-$MX_5$ fragment is tetragonal pyramidal. The origin of this distortion will be analysed at a later point.

**$[Re(NO)_2(P^iPr_3)_2\{ONRe(NO)(P^iPr_3)_2H\}]^+$ $V^+$.** The last complex we include in this section can be described as an adduct of the type $[\mathbf{I}^+]_{V^+}[\mathbf{II}]_{V^+}$ (the nomenclature $[\mathbf{X}]_Y$ stands for a fragment having the structure of **X** but with the geometric parameters as found in the molecule **Y**). It is prepared by the reaction of $[(C_6H_5)_3C][BAr^F_4]$ on **II** in a 1:2 ratio. The geometry in the crystal is displayed in Fig. 6. The oxygen of one of the nitrosyl groups of **II** is apparently a Lewis base strong enough to interact with other Lewis acids, such as $\mathbf{I}^+$ or $BF_3$.[8] The geometry of the $[\mathbf{I}^+]_{V^+}$ fragment is similar to that of **IV**$^+$, and might also be described as a tetragonal pyramid. The bend of one of the NO ligands, however, is not as prominent as in **IV**$^+$, and the L–Re–N angles are also somewhat closer to the value of 120° of the ideal trigonal bipyramid (see Table 1). The geometry of the $[\mathbf{II}]_{V^+}$ fragment is related to that of **II**. A major difference is an even smaller P–Re–P angle of 141°. One of the nitrosyl oxygen atoms of $[\mathbf{II}]_{V^+}$ functions as a Lewis base, which leads to electron depletion at this particular nitrosyl ligand. This in turn can be counteracted by an effective back donation, which is made possible by the narrowing of the P–Re–P angle (see above). We have found a similar effect for the complex [Re(H)(NO)-$(NOBF_3)(P^iPr_3)_2$].[8] The Re and the bridging NO are not coplanar; the Re1–O3–N3–Re2 dihedral angle amounts to 139°.

It was mentioned that the co-ordination geometries of both complexes **IV**$^+$ and **V**$^+$ are closer to a TP than to a TBP co-ordination. To put this argument on more quantitative grounds, we follow the approach of Muetterties,[18] and obtain a measure of shape for these aggregates by means of the dihedral angles $\delta$ formed by the normals to adjacent faces of a given polytopal form. The three five-co-ordinated molecules described for the first time in this work can then be compared to the idealized geometries of a $D_{3h}$ trigonal bipyramid and a $C_{4v}$ tetragonal pyramid, as shown below [adopted from ref. 18(*b*)]. The molecules are oriented such that the phosphorus ligands occupy the $A_1$ and $A_2$ positions. For **III**$^+$, the CO ligand is chosen to occupy the $E_2$ position, whereas for **IV**$^+$ and **V**$^+$ the bent nitrosyl ligand is placed at $E_2$.

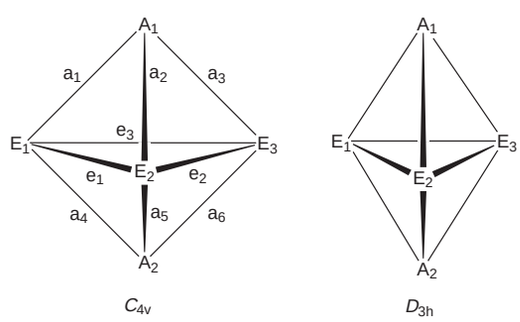


The results of the shape analysis for the rhenium complexes together with values for the ideal co-ordination polyhedra as defined by Muetterties[18] are collected in Table 2. The values of the shape determining angles $\delta(e_n)$, especially that of $\delta(e_3)$, and the fact that two of the $\delta(a_n)$ angles, namely $\delta(a_2)$ and $\delta(a_5)$, are significantly smaller than the remaining members of the set, all indicate that **IV**$^+$ and **V**$^+$ are indeed closer to the $C_{4h}$-TP in co-ordination geometry. For **III**$^+$, the $\delta(a_n)$ angles span a smaller range of values, and its co-ordination geometry is related to that of the $D_{3h}$-TBP. Also, the standard deviations $\sigma(\Gamma)$, eqn. (1), lead to the same conclusion that the co-ordination

$$\sigma(\Gamma) = \sqrt{\frac{1}{9}\sum_{n=1}^{9}((\delta_n)_{exp} - (\delta_n)_\Gamma)^2} \qquad (1)$$

polyhedra for **IV**$^+$ and **V**$^+$ match closer the tetragonal pyramid, and that **III**$^+$ can be described as a trigonal bipyramid (compare Table 2).

## Computational studies

We divide the twelve model complexes as presented in Fig. 1 into two groups. Symmetric complexes $\mathbf{1}^+$–$\mathbf{9}^+$ are characterized by ligands L, which possess higher symmetry than $C_s$, whereas

§ The principal orbital interactions for five- and six-co-ordination have been investigated by Hoffmann and co-workers in a classical series of papers, see refs. 15 and 17.

**Table 3** Optimized geometries[a] for $C_s$-symmetric $[Re(NO)_2(PH_3)_2L]^{n+}$ model complexes ($n = 0$ or 1)

| Complex | L | Re–L | Re–P | Re–N | N–O | P–Re–P | Re–N–O | N–Re–N | Other | |
|---|---|---|---|---|---|---|---|---|---|---|
| $\mathbf{1}^+$ | — | — | 245.7 | 180.3 | 118.3 | 160.8 | 161.9 | 118.5 | | |
| **2** | $H^-$ | 172.4 | 239.1 | 182.5 | 120.3 | 151.7 | 174.1 | 126.6 | | |
| $\mathbf{3}^+$ | CO | 200.9 | 247.0 | 183.9 | 117.6 | 174.0 | 175.2 | 125.9 | C–O | 115.3 |
| $\mathbf{4}^+$ | $CNCH_3$ | 206.5 | 245.4 | 183.0 | 118.3 | 173.2 | 172.8 | 123.1 | C–N | 117.2 |
| $\mathbf{5}^+$ | $PH_3$ | 248.8 | 245.6 | 182.4 | 118.4 | 176.1 | 169.9 | 121.6 | H–P–H | 98.2 |
| **6** | $CN^-$ | 210.7 | 242.5 | 182.2 | 119.9 | 160.9 | 171.7 | 121.6 | C–N | 117.6 |
| $\mathbf{7}^+$ | $NCCH_3$ | 213.8 | 245.7 | 181.5 | 118.7 | 173.5 | 168.3 | 116.9 | N–C | 116.3 |
| **8** | $Cl^-$ | 249.2 | 243.3 | 180.7 | 120.4 | 161.2 | 166.6 | 115.1 | | |
| $\mathbf{9}^{+b}$ | ON | 216.6 | 247.9 | 181.1 | 118.2 | 172.6 | 166.5 | 110.9 | O–N | 119.4 |
| | | | 247.7 | 180.7 | 118.1 | | 167.0 | | Re–O–N | 179.5 |

[a] Distances in pm, angles in °. [b] Unrestricted calculation without symmetry constraints on the doublet state.

**Table 4** Optimized geometries[a] for asymmetric $[Re(NO)_2(PH_3)_2L]^+$ complexes

| Complex | L | Re–L | Re–P | Re–N | N–O | P–Re–P | Re–N–O | N–Re–N | Other | |
|---|---|---|---|---|---|---|---|---|---|---|
| $\mathbf{10}^+$ | $H_2CO$ | 222.0 | 246.1 | 179.3 | 118.2 | 167.7 | 176.9 | 108.5 | C–O | 123.5 |
| | | | | 184.6 | 119.3 | | 147.8 | | L–Re–N | 95.3; 156.2 |
| *trans*-$\mathbf{11}^+$ | ONH | 211.2 | 247.4 | 182.5 | 118.2 | 176.8 | 164.6 | 121.5 | O–N | 126.6 |
| | | | | 181.7 | 118.6 | | 172.6 | | O–N–H | 104.4 |
| | | | | | | | | | L–Re–N | 115.6; 122.9 |
| *cis*-$\mathbf{11}^+$ | ONH | 211.2 | 247.6 | 180.8 | 119.1 | 169.9 | 145.8 | 109.6 | O–N | 125.2 |
| | | | | 185.9 | 118.3 | | 180.0 | | O–N–H | 107.1 |
| | | | | | | | | | L–Re–N | 156.9; 93.5 |
| $\mathbf{12}^+$ | ONR′[b] | 222.2 | 245.0 | 179.3 | 119.1 | 160.6 | 177.7 | 108.2 | O–N | 126.0 |
| | | | | 183.9 | 119.5 | | 149.4 | | L–Re–N | 154.3 |
| | | | | | | | | | | 97.5 |
| | | | | | | | | | O–N–R′ | 126.0 |

[a] Distances in pm, angles in °. [b] R′ = $Re(NO)(PH_3)_2H$.

in the asymmetric complexes $\mathbf{10}^+$–$\mathbf{12}^+$ the ligands are considered to be mirror symmetric. Selected geometric parameters are presented in Tables 3 and 4, respectively. If we compare the optimized geometries of compounds $\mathbf{1}^+$, **2** and $\mathbf{3}^+$ with the crystal structures of $\mathbf{I}^+$, **II** and $\mathbf{III}^+$ we find reasonable agreement between experiment and theory. The general trends are well reproduced in the calculations, *e.g.* a shortening of Re–P and an increase in N–Re–N when going from $\mathbf{I}^+(\mathbf{1}^+)$ to **II**(**2**). The Re–N separation is generally overestimated in the calculations by about 6 pm. As a consequence, due to a reduced back bonding, the N–O distance falls somewhat short in comparison to the experiment. Surprisingly, the simple model phosphine $PH_3$ reproduces the co-ordination geometry of the phosphorus ligands extremely well, especially where the Re–P distances are concerned. Also, $\mathbf{10}^+$ and $\mathbf{12}^+$ seem to be good models for complexes $\mathbf{IV}^+$ and $\mathbf{V}^+$, respectively. The calculation predicts the asymmetric co-ordination with two different nitrosyl ligands as found in the experiment. The co-ordination geometry of the nitrosyl ligand is in satisfactory accordance to the crystal structure, and the angles P–Re–O and N–Re–N are also close to within 2°.

**Influence of the phosphorus donor.** The reasonable close agreement between the calculated and observed P–Re–P angle of the symmetric complexes suggests that this parameter is not overly dependent on the nature of the R group of the $PR_3$ ligand. Instead, the right polarization of the $d_{xz}$ orbital needed to achieve an optimum ratio of back bonding between the NO and L ligands to first order determines the degree of $PR_3$ bending (see above). The different donor capability however influences the electron densities at the Re, and therefore to a certain extent the geometric arrangement of the ligands in the *yz* plane. This might explain the somewhat larger deviation between theory and experiment in the Re–N distances.

We further checked the influence of the P–Re–P angle on the co-ordination of the NO and L ligands by restricted geometry optimizations for complexes $\mathbf{1}^+$–**8**, in which P–Re–P was fixed at 150 and 170°, respectively. In all cases, only marginal geometric differences compared to the fully optimized species were found. The potential energy surface for the P–Re–P bend is very shallow, and the angle bending does not require much energy. As an example, we provide two cases, beginning with **2**, the angle P–Re–P fixed at 170°. For the 18° distortion from the calculated equilibrium geometry, an energy of only 11 kJ $mol^{-1}$ is needed. The average deviation between selected bond distances and angles amounts to 0.4 pm and 1.0°. For $\mathbf{5}^+$ fixed at 150°, narrowing the P–Re–P requires 38 kJ $mol^{-1}$. The selected angles change on average by 0.6°, and the bond distances (Re–L excluded) by 0.3 pm. The Re–L bond in $\mathbf{5}^+$ (150°) is elongated by 3.2 pm. This is easily explained by keeping in mind that diminishing the P–Re–P angle leads to a polarization of $d_{xz}$ away from L, and thus to a reduced back bonding to the $PH_3$ ligand in equatorial position. This in turn weakens and lengthens the P–Re bond.

Additional information on structures and energies of the restricted geometry complexes can be found in SUP 57540.

The P–Re–P size allows us to weigh the importance of $\pi_{xz}$ back bonding to L. For $[Re(NO)_2(PR_3)_2L]$ complexes in which P–Re–P is about the same size or smaller than in the $Re(NO)_2(PR_3)_2$ fragment, this back-bonding interaction is of no or only minor importance. This is naturally the case for $L = H^-$, **2**, and $Cl^-$, **8**, but also for $CN^-$, **6**. On the other hand, when P–Re–P is substantially larger than in the free fragment, $\pi_{xz}$ back bonding is of importance, as it is for L = CO, $\mathbf{3}^+$, $CNCH_3$, $\mathbf{4}^+$, $NCCH_3$, $\mathbf{7}^+$, and also for $PH_3$, $\mathbf{5}^+$. This argument is based on qualitative considerations, and it does not allow one to infer direct correlation between the amount of π back bonding and the P–Re–P angle. Re-$d_{xz}$ Interactions with other ligand based orbitals, as well as interactions involving Re-$d_{yz}$, further influence P–Re–P and the amount of π back donation to the equatorial ligands.

**Dependence of the angle N–Re–N on the nature of L.** We already mentioned the important orbital interactions which determine the size of N–Re–N in relation to the problem of the ground state geometry of $[Re(NO)_2(PCy_3)_2]^+$ $\mathbf{I}^+$. We will now

**Table 5** Composition of the three highest occupied orbitals of the complexes **2**, $\mathbf{3}^+$ and **8** at their equilibrium geometry

| Complex | Symmetry | Re (%) | | | NO (%) | | | | L (%) | |
|---|---|---|---|---|---|---|---|---|---|---|
| **2** | $1b_1$ | $p_x$ 5 | $d_{xz}$ 48 | $d_{x^2-y^2}$ 8 | N $p_x$ 9 | | O $p_x$ 24 | | | |
| | $1a_1$ | $p_z$ 11 | $d_{z^2}$ 7 | | N $p_y$ 8 | N $p_z$ 13 | O $p_y$ 16 | O $p_z$ 21 | H s 9 | |
| | $1b_2$ | $p_y$ 9 | $d_{yz}$ 31 | | N $p_z$ 15 | | O $p_z$ 29 | | | |
| $\mathbf{3}^+$ | $1b_1$ | | $d_{xz}$ 60 | $d_{x^2-y^2}$ 5 | N $p_x$ 5 | | O $p_x$ 14 | | C $p_x$ 3 | O $p_x$ 6 |
| | $1a_1$ | $p_z$ 9 | $d_{z^2}$ 18 | | N $p_y$ 8 | N $p_z$ 13 | O $p_y$ 15 | O $p_z$ 22 | C s 3 | C $p_z$ 1 |
| | $1b_2$ | $p_y$ 9 | $d_{yz}$ 34 | | N $p_z$ 12 | | O $p_z$ 22 | | C $p_y$ 5 | O $p_y$ 7 |
| **8** | $1b_1$ | | $d_{xz}$ 37 | $d_{x^2-y^2}$ 7 | N $p_x$ 7 | | O $p_x$ 19 | | Cl $p_x$ 32 | |
| | $1a_1$ | $p_z$ 6 | $d_{z^2}$ 19 | | N $p_y$ 9 | N $p_z$ 6 | O $p_y$ 25 | O $p_z$ 13 | Cl $p_z$ 12 | |
| | $1b_2$ | $p_y$ 7 | $d_{yz}$ 19 | | N $p_y$ 6 | N $p_z$ 15 | O $p_y$ 11 | O $p_z$ 22 | Cl $p_y$ 13 | |

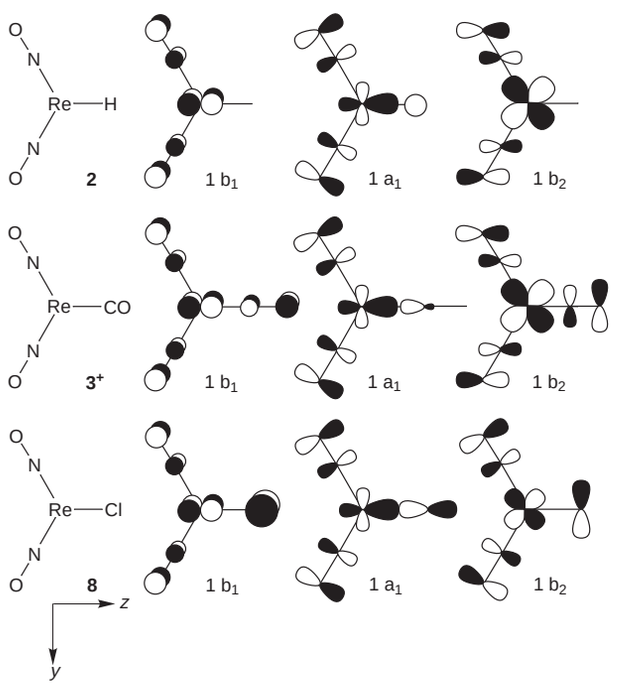


**Fig. 7** Sketches of the three highest molecular orbitals of complexes **2**, $\mathbf{3}^+$ and **8**. Not shown are contributions due to the phosphorus donor ligands.

discuss this structural parameter in more detail, and address the question how different types of ligands L may influence N–Re–N in $[Re(NO)_2(PR_3)_2L]^{n+}$ complexes. We have chosen L to be a σ donor, π acceptor, or a π donor ligand. The representative model compounds which we will analyse in detail are then **2**, $\mathbf{3}^+$ and **8**.

The highest three occupied molecular orbitals for these complexes are displayed in Fig. 7. The basic composition of these MOs is similar in all three compounds, and a detailed breakdown is presented in Table 5. The metal contribution to the HOMO-2, $1b_1$, is mainly Re-$d_{xz}$. Back bonding to the $\pi^*_{NO,xz}$ orbitals increases, when P–Re–P is diminished, and $1b_1$ is lowered in energy. There is no contribution from $H^-$ to $1b_1$ in **2**. For $\mathbf{3}^+$ a $\pi^*_{CO,xz}$ acceptor orbital is combined with Re-$d_{xz}$ in a bonding fashion, whereas for **8** we have antibonding interaction between the metal based orbital and a filled $p_{x,Cl^-}$ orbital. Not shown in Fig. 7 are contributions of the $PH_3$ ligand to $1b_1$. Their importance has been discussed in the previous sections.

In orbital $1a_1$ back bonding occurs from the metal Re-$d_{z^2}$ to the $\pi^*_{NO,yz}$ orbitals. Again, the overlap increases when P–Re–P becomes smaller. The contributions from L to $1a_1$ are in all cases σ antibonding; the ligand orbitals involved are $s_{H^-}$ **2**, $\sigma_{CO}$ $\mathbf{3}^+$ and $p_{z,Cl^-}$ **8**.

Lastly, back bonding to $\pi^*_{NO,yz}$ is also possible from Re-$d_{yz}$, as realized in $1b_2$. In contrast to $1a_1$, the overlap is now lessened when P–Re–P decreases. As in the case of $1b_1$, there is no contribution from $H^-$, **2**, a bonding interaction with $\pi^*_{CO,yz}$, $\mathbf{3}^+$, and an antibonding interaction with $p_{y,Cl^-}$, **8**.

Our analysis shows that two metal d orbitals compete for back bonding to the $\pi^*_{NO,yz}$ orbitals, namely $d_{z^2}$ in $1a_1$ and $d_{yz}$ in $1b_2$.¶ However, these interactions show a different nature in their dependence on the angle N–Re–N. In the former case the metal–ligand overlap increases when N–Re–N decreases, whereas for the latter the opposite trend holds. The relative importance of these two interactions will determine the size of N–Re–N.

The Walsh diagram along the N–Re–N bending mode for the three highest occupied orbitals for complexes **2**, $\mathbf{3}^+$ and **8** is displayed in Fig. 8. The energy curve for orbital $1b_1$ looks similar in all three cases; the interaction of $d_{xz}$ with $\pi^*_{NO,xz}$ is mainly influenced by the phosphorus donors, and only to a minor degree by the nature of the ligand L. This orbital serves as a reference point for the comparison of the relative energies of the orbitals amongst the different systems (due to the cationic nature of $\mathbf{3}^+$, its orbitals are at considerably lower energies than those of **2** and **8**). The energy dependence of $1a_1$ and $1b_2$ follows the expected trend in all three cases, but there are some important differences. For **2**, we find orbital crossing of $1a_1$ and $1b_2$ around 120°, close to the value of N–Re–N in the "free" fragment $\mathbf{1}^+$. Distortion of this angle leads to a stabilization of the HOMO-1, which is $1a_1$ when N–Re–N decreases, or $1b_2$ when N–Re–N increases. The orbital coefficient of the metal based d orbitals in $1a_1$ is smaller when compared to Re-$d_{yz}$ in $1b_2$. In the case of $1a_1$, this is due to the antibonding interaction between the d orbitals and $s_{H^-}$. Consequently, back bonding is more efficient in $1b_2$, and when complex **2** is formed from the fragments N–Re–N will open up to lower the energy of $1b_2$, and to increase this particular interaction.

We encounter a similar situation for complex $\mathbf{3}^+$. Again, we see the destabilizing σ interaction in $1a_1$, which leads to orbital crossing at around 120°. Again, the metal d contributions are smaller in $1a_1$ than in $1b_2$, so that an increase in N–Re–N maximizes the bonding energy.

The picture emerged so far changes, when considering the π donor $Cl^-$. In complex **8** both orbitals $1a_1$ and $1b_2$ undergo antibonding interaction with occupied $p_{Cl^-}$ orbitals; $1b_2$ is significantly destabilized when compared to $1a_1$, and the orbital crossing occurs at an angle of around 135°, far from the free fragment. At the N–Re–N value of $\mathbf{1}^+$, orbital $1a_1$ now provides the main backbonding interaction, so that in this case N–Re–N is diminished, to maximize overlap and bonding energy.

To sum up our analysis, we might say that in $[Re(NO)_2(PR_3)_2L]^{n+}$ complexes, when L is a pure σ donor or a π acceptor, the value of N–Re–N is larger than that of the free fragment $[Re(NO)_2(PR_3)_2]^+$. In contrast, if L is a π donor, we expect to find a decrease in N–Re–N. This might allow us to judge the relative importance of π acceptor *vs.* π donor interaction. From

¶ Strictly speaking, the metal d contribution in $1a_1$ is a mixture of $d_{z^2}$ and $d_{x^2-y^2}$, and in complex **2** both components are of equal importance. For the sake of convenience, we keep referring to $d_{z^2}$ in the $1a_1$ case since only this orbital participates in the σ antibonding interaction with L; further details are to be found in Table 4.

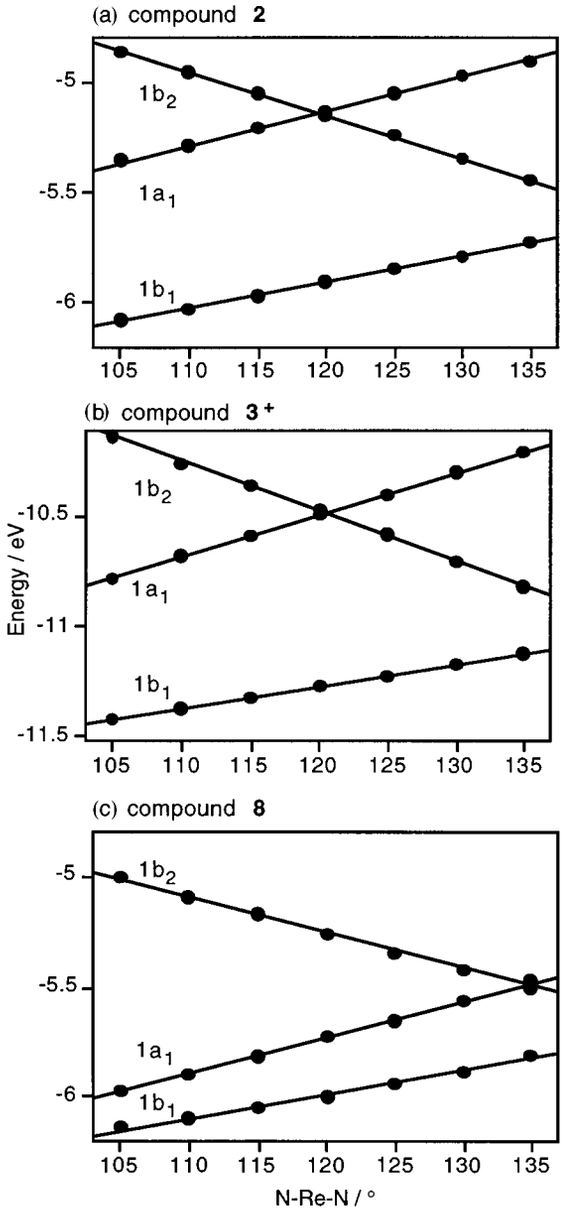


**Fig. 8** Walsh diagram along the N–Re–N bending mode for (a) complex **2**, (b) $\mathbf{3}^+$ and (c) **8**.

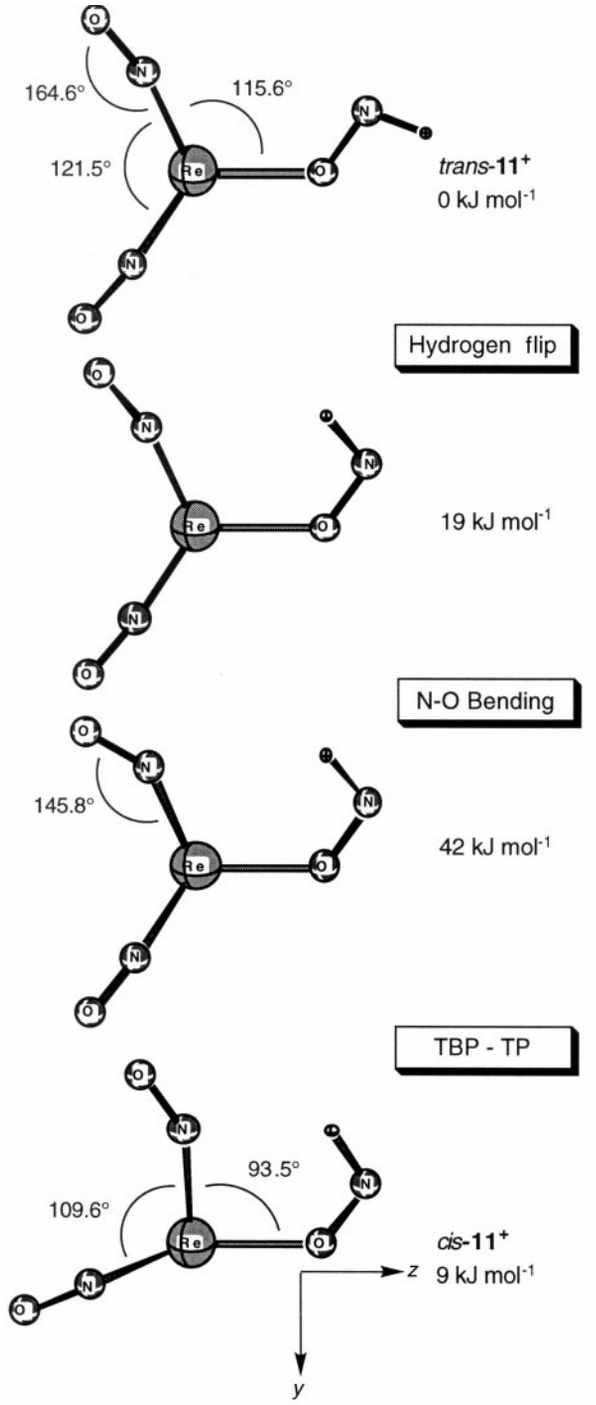


**Fig. 9** Molecular structures along the transformation pathway *trans*-$\mathbf{11}^+ \longrightarrow$ *cis*-$\mathbf{11}^+$. The $PH_3$ groups are omitted for clarity. See text for further details.

the values presented in Table 2, we see that, in addition to $H^-$ and CO, $NCCH_3$, $PH_3$ and $CN^-$ also show an increase in N–Re–N. Interestingly, for the acetonitrile complex we find a smaller value for this angle, which might indicate that in this case π-acceptor interaction is of only minor importance. The same holds true for the isonitrosyl ligand N*O*.

Before continuing our discussion, we should explain why we included the somewhat unusual isonitrosyl ligand in the list of our model compounds. Initially, we wanted to find a simple model for complex $\mathbf{V}^+$ in order to investigate the nature of the NO bend and the unusual co-ordination geometry. To probe the influence of π donation on the co-ordination geometry of the nitrosyl ligands, we provided for starting geometries **8** and $\mathbf{9}^+$, in which the $Re(NO)_2(PR_3)_2$ fragment adapted a similar arrangement to that found in the crystal structures of $\mathbf{IV}^+$ and $\mathbf{V}^+$. All attempts to optimize such an asymmetric structure, however, converged to the symmetric co-ordination geometry of **8** or $\mathbf{9}^+$. This was a first indication that no orbital effect is probably responsible for the particular co-ordination geometry of $\mathbf{V}^+$. We then extended our calculations to the asymmetric complexes $\mathbf{10}^+$–$\mathbf{12}^+$, and also considered steric effects in our analysis. These results are presented in the next paragraph.

**Origin of the NO bend.** The formaldehyde compound $\mathbf{10}^+$ already provides a good model of the benzaldehyde complex $\mathbf{IV}^+$. The calculation satisfactorily reproduces the main structural features of the experimentally determined structure. One of the NO ligands is bent by about 30°, and the co-ordination geometry falls between TBP and TP (see data in Tables 1 and 4). The calculations on the hypothetical nitroso hydride[19] complex $\mathbf{11}^+$ provide an initial clue as to why one of the NO ligands deviates from a linear co-ordination geometry. For HNO two different co-ordination geometries are possible, the first in which the hydrogen points away from the metal fragment, *trans*-$\mathbf{11}^+$, a second in which it is directed toward one of the NO ligands, namely *cis*-$\mathbf{11}^+$. As can be seen from the data in Table 4, *trans*-$\mathbf{11}^+$ adopts a co-ordination geometry close to that of TBP,

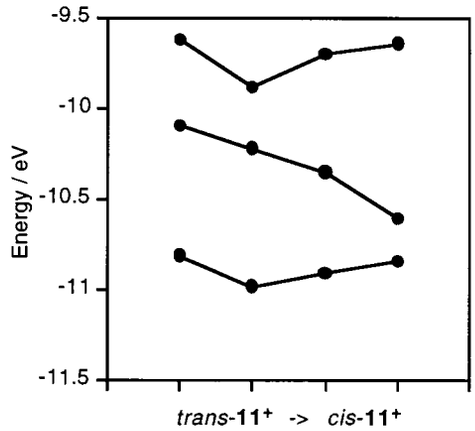


**Fig. 10** Orbital energy diagram for the three highest occupied orbitals along the path *trans*-**11**$^+$ ⟶ *cis*-**11**$^+$.

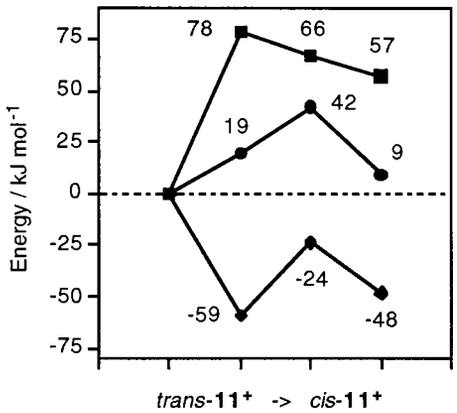


**Fig. 11** Energy decomposition along the path *trans*-**11**$^+$ ⟶ *cis*-**11**$^+$. The total bonding energy (●, TBE) is divided into steric (■, $\Delta E^0$) and electronic (◆, $\Delta E_{int}$) contributions. See text for further details.

whereas *cis*-**11**$^+$ displays the distorted TBP–TP arrangement, as found in **10**$^+$ or **IV**$^+$ (see also Fig. 9).

To analyse the origin of this distortion we performed calculations for hypothetical molecules on the pathway *trans*-**11**$^+$→ *cis*-**11**$^+$. Beginning with the fully optimized geometry of *trans*-**11**$^+$, we introduce a hydrogen flip by a 180° rotation around the ON axis of the nitroso hydride ligand, while keeping all other geometric parameters fixed. We then allow for the NO bend to adapt to the value of *cis*-**11**$^+$. Finally we let the complex relax to the fully optimized asymmetric geometry *cis*-**11**$^+$. This transformation is illustrated in Fig. 9. The corresponding orbital energy diagram of the highest three occupied orbitals is presented in Fig. 10.

In light of this analysis it appears as though the symmetric *cis* structure should be the most stable one, and the geometry distortion to the final structure of *cis*-**11**$^+$ should not seem obvious. As anticipated, no orbital effect is clearly responsible for the observed modification in complex geometry when the co-ordination of the HNO ligand is changed from *trans* to *cis*. We extended our analysis also to include steric effects, and essentially decomposed the total bonding energy TBE of a given molecule into components due to repulsive steric interaction, $\Delta E^0$, and attractive orbital interaction, $\Delta E_{int}$.[20] The energy decomposition along the pathway *trans*-**11**$^+$→*cis*-**11**$^+$ is presented in Fig. 11.

The energy contributions of *trans*-**11**$^+$ are set at zero. Hydrogen flipping leads to an energetic stabilization due to electronic interactions. As can be observed in Fig. 10, all the three $d_{xz}$, $d_{yz}$ and $d_{z^2}$ orbitals are lowered in energy.‖ However, we also find a considerable increase in steric repulsion, so that, as a net effect, the hydrogen flip destabilizes the molecular arrangement by 20 kJ mol$^{-1}$. The NO bend now decreases the steric repulsion from 78 to 66 kJ mol$^{-1}$. The orbital interaction energy however is diminished, since the now partially oxidized metal center has an unfavorable TBP co-ordination geometry. In the last step the geometry relaxes from TBP to TP, which effectively enhances the electronic interaction and further reduces the steric repulsion.

Our analysis shows that the hydrogen of the HNO ligand, when pointing towards one nitrosyl group, leads to an increase in $\Delta E^0$. Bending of the affected NO minimizes steric repulsion, and further rearrangement to the TP geometry maximizes electronic interaction. The same structural element, a hydrogen pointing toward a nitrosyl ligand, can be found in the case of the formaldehyde or benzaldehyde ligands in **10**$^+$ or **IV**$^+$, respectively. This hydrogen then induces the same structural changes discussed for the hypothetical nitroso hydride complex **11**$^+$.

The last question we want to address is whether or not steric repulsion is also responsible for the geometric distortion encountered in complex **V**$^+$. To this end, we performed a bonding analysis of the model compound **12**$^+$, by building up the final complex from the constituting fragments **1**$^+$ and **2**, eqn. (2). The energy associated with eqn. (2) is the so-called

$$\underset{\mathbf{2}}{H(NO)(PH_3)_2ReNO} + \underset{\mathbf{1}^+}{[Re(NO)_2(PH_3)_2]^+} \longrightarrow \underset{\mathbf{12}^+}{[H(NO)(PH_3)_2ReNO{\rightarrow}Re(NO)_2(PH_3)_2]^+} \quad (2)$$

bond snapping energy $BE_{snap}$,[21] since the fragments have already been promoted from their ground state geometry to the one they adopt in the final complex; $BE_{snap}$ can again be broken down into steric and electronic contributions, eqn. (3). The

$$BE_{snap} = -[\Delta E^0 + \Delta E_{int}] \quad (3)$$

bond analysis was performed not only for **12**$^+$, but for a symmetrical compound *sym*-**12**$^+$ as well, which was constructed by adopting structural features from **12**$^+$ [geometry of the $H(NO)(PH_3)_2ReNO$ fragment and the phosphorus donor ligands, N–Re–N] and **9**$^+$ (O–N–Re). The geometries of both model complexes are shown in Fig. 12, and the results of the bonding analysis are collected in Table 6. For the two co-ordination geometries the electronic interaction energy is virtually identical. Again, a reduced steric repulsion in **12**$^+$ favors the Re–L bond in the asymmetric compound by 16 kJ mol$^{-1}$.

In this section we have elucidated the role of $\Delta E^0$ in the co-ordination geometry of $[Re(NO)_2(PR_3)_2L]^{n+}$ complexes. In asymmetric co-ordination geometries one of the NO ligands bends to reduce steric repulsion between $[Re(NO)_2(PR_3)_2]^+$ and the ligand L. Noteworthy is the fact that this bending distortion does not require much energy; $\Delta E_{bend}$ can be estimated as about 20 kJ mol$^{-1}$. The NO ligand seems to be very flexible in adapting to the right co-ordination geometry and effectively minimizing steric repulsion; this is evident not only in the TBE–TP geometries of **IV**$^+$ and **V**$^+$, but also in the strong cisoid bends encountered in **I**$^+$.

## Conclusion

The co-ordination chemistry of the 16e$^-$ fragment $[Re(NO)_2(PR_3)_2]^+$ **1**$^+$ has been explored by means of crystal structure analyses and DFT calculations. The ion possesses a $C_{2v}$ butterfly ground state geometry. This arrangement could be

‖ We adopt a simplified classification of the orbitals according to the Re-d contributions. To not confuse the reader, we prefer to keep the nomenclature as it was established for $C_{2v}$ symmetry, although the correct classification for the HOMO to HOMO-2 should be $d_{x^2-y^2}$, $d_{xy}$ and $d_{yz}$. Furthermore, in some cases we have substantial mixing between $d_{x^2-y^2}$ and $d_{xy}$.

**Table 6** Bond analyses[a] for the model complexes $\mathbf{12}^+$ and *sym*-$\mathbf{12}^+$

| | $\mathbf{12}^+$ | *sym*-$\mathbf{12}^+$ |
|---|---|---|
| $DE^0$ | 38 | 54 |
| $DE_{int}$ | −213 | −212 |
| $BE_{snap}$ | 175 | 158 |

[a] In kJ $mol^{-1}$.

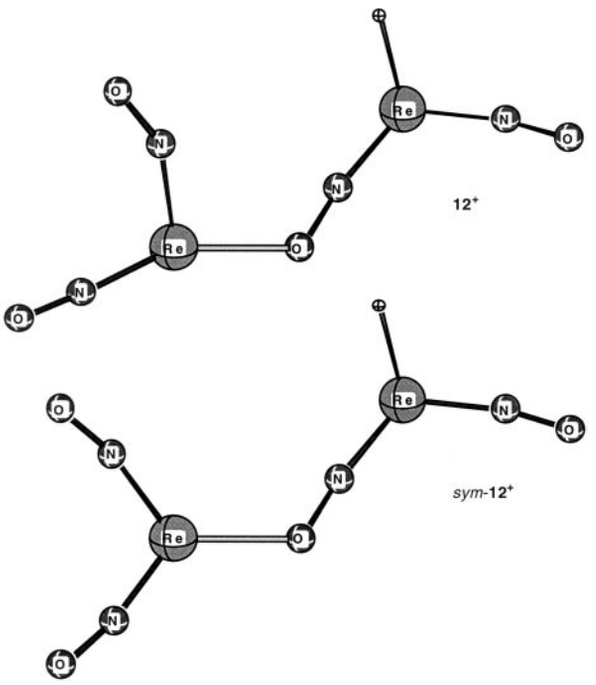


**Fig. 12** Molecular structures of complex $\mathbf{12}^+$ and *sym*-$\mathbf{12}^+$ in the plane of the NO ligands; $PH_3$ groups are omitted for clarity.

rationalized by simple arguments based on orbital interactions, similar to those employed for the isoelectronic compound $[Ru(CO)_2(P^tBu_2Me)_2]$.[13] The structural changes of the $[Re(NO)_2(PR_3)_2]^+$ under formation of $[Re(NO)_2(PR_3)_2L]^{n+}$ complexes ($n = 0$ or 1) have been used to characterize the nature of the Re–L bond. The angle P–Re–P is determined by the competition for π-back bonding between the nitrosyl groups and the ligand L. In symmetric complexes a new orbital effect was found to determine the size of the N–Re–N angle. When L is a pure σ donor or π acceptor the value of N–Re–N is larger than that of $\mathbf{1}^+$. In contrast, if L is a π donor, we expect to find a decrease in N–Re–N. In asymmetric complexes it was shown that the driving force in bending of one of the NO groups and the subsequent distortion from a TBP to a TBP–TP is the minimization of steric repulsion. We have also seen that this rearrangement is accompanied by only small changes in the bonding energy, and that the NO ligand is very flexible in adapting its co-ordination geometry to changes in electronic structure or steric influences. This might entail important implications for the chemistry and reactivity of $\mathbf{1}^+$.

In this work we have investigated the structural and static features of the co-ordination chemistry of the $[Re(NO)_2(PR_3)_2]^+$ fragment. This study is intended to provide a basis for a better understanding of the reactivity and dynamic features of this transition metal complex. We are currently investigating the potential of $\mathbf{1}^+$ as an effective catalyst in hydrogenation and hydrosilation reactions.[22] From a theoretical point of view, the nature of the intramolecular interaction between the bending nitrosyl groups and the ligand L provides an interesting challenge. Further investigations might reveal whether or not intramolecular hydrogen bonding can indeed be related to the phenomenon of NO bending.

## Experimental

All operations were carried out under a nitrogen atmosphere using standard Schlenk and glove-box techniques. Solvents were dried over sodium diphenylketyl [THF, $Et_2O$, $O(SiMe_3)_2$, hydrocarbons] or $P_2O_5$ ($CH_2Cl_2$) and distilled under $N_2$ prior to use. The deuteriated solvents used in the NMR experiments were dried over sodium diphenylketyl ($C_6D_6$, toluene-$d_8$, THF-$d_8$) or $P_2O_5$ ($C_6D_5Cl$, $CD_2Cl_2$) and vacuum transferred for storage in Schlenk flasks fitted with Teflon stopcocks.

All NMR experiments were carried out on a Varian Gemini 300 spectrometer. Chemical shifts are given in ppm. The $^1H$ and $^{13}C$-{$^1H$} NMR spectra were referenced to the residual proton or $^{13}C$ resonances of the deuteriated solvent, $^{31}P$ chemical shifts externally referenced to 85% $H_3PO_4$ sealed in a capillary and inserted into a standard 5 mm NMR tube filled with the deuteriated solvent. The IR spectra were recorded on a Bio-Rad FTS-45 spectrometer.

The complex $[Re(NO)_2(P^iPr_3)_2H]$ **II** was prepared according to a reported procedure.[9] Benzaldehyde was purchased from Fluka (puriss.), degassed and used without further purification.

For the crystal structure analyses, the diffraction data were collected on an image plate detector system (STOE IPDS) for complexes $\mathbf{I}^+$ and $\mathbf{III}^+$, and on a four circle diffractometer (upgraded Nicolet R3) for $\mathbf{IV}^+$ and $\mathbf{V}^+$. The X-ray generators were equipped with sealed tubes and graphite monochromators (Mo-Kα, $\lambda = 0.71073$ Å). All crystals were mounted on glass rods or on top of glass capillaries using silicon grease ($\mathbf{IV}^+$, $\mathbf{V}^+$) or covered with perfluoro polyether oil ($\mathbf{I}^+$, $\mathbf{III}^+$). Programs used for cell refinement, data collection and data reduction: CELL,[23] EXPOSE,[23] INTEGRATE,[23] XRED[23] and XDISK;[24] for absorption correction, numerical,[25] XRED ($\mathbf{I}^+$, $\mathbf{III}^+$), and semiempirical based on ψ-scan data, XEMP ($\mathbf{V}^+$).[24] Structure solution was done with SHELXS 97[26] ($\mathbf{I}^+$, $\mathbf{III}^+$) and SIR 92[27] ($\mathbf{IV}^+$, $\mathbf{V}^+$). Structure refinement was done with SHELXL 97[28] ($\mathbf{I}^+$, $\mathbf{III}^+$) and CRYSTALS 96[29] ($\mathbf{IV}^+$, $\mathbf{V}^+$). All positions of the hydrogen atoms, except for the hydride of $\mathbf{V}^+$, were calculated at distances relevant for the measuring temperature, and were placed geometrically for each refinement cycle. Complexes $\mathbf{I}^+$ and $\mathbf{III}^+$ were refined on $F_o^2$ using all unique reflections, applying an empirical weighting scheme;[28] $\mathbf{IV}^+$ and $\mathbf{V}^+$ were refined on $F_o$ using reflections with $I > \sigma(I)$, and a Chebyshev polynomial weighting scheme.[30] Molecular graphics were done with PLATON 97.[31]

CCDC reference number 186/1421.

See http://www.rsc.org/suppdata/dt/1999/1717/ for crystallographic files in .cif format.

### Preparations

**$[Re(NO)_2(PCy_3)_2][BAr^F_4]$.** A heterogeneous mixture containing $[Re(NO)_2(PCy_3)_2H]$ (150 mg, 0.189 mmol) and $[Ph_3C][BAr^F_4]$ (209 mg, 0.189 mmol) in $C_6H_6$ (15 mL) was stirred for 2 h. During this period a dark red oily solid forms. The solvent was removed *in vacuo* until *ca.* 3 mL of $C_6H_6$ were left, and then pentane was added (15 mL). The liquid was discharged and the solid washed with additional pentane (3 × 15 mL) and dried *in vacuo* to give 290 mg of $\mathbf{I}^+[BAr^F_4]$ (91.9%). Crystals for the X-ray diffraction study were grown by cooling slowly, starting at 90 °C, a saturated $C_6H_6$ solution of the complex. IR(Nujol): $\nu_{NO}$ 1711m and 1649s $cm^{-1}$. $^{31}P$-{$^1H$} NMR ($C_6D_5Cl$): $\delta$ 46.5 (s). $^1H$ NMR ($C_6D_5Cl$): $\delta$ 8.10 (m, br, 8 H, $BAr^F_4$), 7.47 (m, br, 4 H, $BAr^F_4$) and 2.30–0.6 (m, 66 H, $PCy_3$) (Calc. for $C_{68}H_{78}BF_{24}N_2O_2P_2Re$: C, 48.90; H, 4.71; N, 1.68. Found: C, 48.72; H, 4.65; N, 1.57%).

*Crystal structure determination.* The compound crystallizes with one molecule of $C_6H_6$ and one molecule of $(C_2H_5)_2O$ per unit cell, which are both disordered *via* a center of symmetry. Thus, the solvent molecules were refined isotropically. $C_{73}H_{86}BF_{24}N_2O_{2.5}P_2Re$, $M = 1746.39$, triclinic, space group $P\bar{1}$ (no. 2), $a = 13.4230(14)$, $b = 17.641(2)$, $c = 17.946(2)$ Å, $\alpha = 101.790(13)$,

$\beta = 109.224(12)$, $\gamma = 92.608(13)°$, $V = 3898.4(0.8)$ Å$^3$ (5000 reflections used for cell parameter refinement), $T = 193$ K, $Z = 2$, $\mu$(Mo-K$\alpha$) = 1.7 mm$^{-1}$, 218 images exposed using a $\varphi$ oscillation scan mode at constant times of 3.0 min per image. 35186 Reflections measured ($\theta_{max} = 26°$), 13856 unique ($R_{int} = 0.0463$) which were used in all calculations, 934 parameters in full matrix refinement, final $R1 = 0.0738$, $wR2(F^2) = 0.1864$.

**[Re(NO)$_2$(PCy$_3$)$_2$(CO)][BAr$^F_4$].** The complex [Re(NO)$_2$(PCy$_3$)$_2$][BAr$^F_4$] (48 mg, 0.0287 mmol) was introduced in a 100 mL flask and $C_6H_6$ (10 mL) added. The mixture was placed under 950 mbar of CO and heated at 80 °C for 10 min. Upon cooling to room temperature small yellow crystals started to be formed. The solvent was removed until *ca*. 1 mL of $C_6H_6$ was left, and then pentane was added (10 mL). The solid was subsequently washed with pentane (2 × 10 mL) and dried under vacuum to give 35 mg of **III**$^+$[BAr$^F_4$] (71.3%). Suitable crystals for the X-ray diffraction study and elemental analyses were obtained by recrystallization in $CH_2Cl_2$–pentane. IR($CD_2Cl_2$): $\nu_{CO}$ 2025m; $\nu_{NO}$ 1717m and 1675s cm$^{-1}$. $^{31}$P-{$^1$H} NMR ($CD_2Cl_2$): $\delta$ 23.6 (s). $^1$H NMR ($CD_2Cl_2$): $\delta$ 7.73 (m, br, 8 H, BAr$^F_4$), 7.60 (m, br, 4 H, BAr$^F_4$) and 2.40–0.8 (m, 66 H, PCy$_3$). $^{13}$C-{$^1$H} NMR ($CD_2Cl_2$): $\delta$ 202.4 (t, CO, $J_{CP} = 9.4$ Hz) (Calc for $C_{69}H_{78}BF_{24}N_2O_3P_2Re$: C, 48.80; H, 4.63; N, 1.65. Found: C, 49.11; H, 4.42; N, 1.58%).

*Crystal structure determination* The compound crystallizes with one molecule of $CH_2Cl_2$ per unit cell, which is disordered *via* a center of symmetry. For the solvent molecule, the split Cl atoms were refined anisotropically, whereas the remaining atoms were treated isotropically. $C_{69.5}H_{79}BClF_{24}N_2O_3P_2Re$, $M = 1740.75$, triclinic, space group $P\bar{1}$ (no. 2), $a = 12.9909(12)$, $b = 16.6700(16)$, $c = 19.0701(19)$ Å, $\alpha = 79.633(12)$, $\beta = 71.952(11)$, $\gamma = 79.440(11)°$, $V = 3826.4(0.6)$ Å$^3$ (5000 reflections used for cell parameter refinement), $T = 193$ K, $Z = 2$, $\mu$(Mo-K$\alpha$) = 1.768 mm$^{-1}$, 200 images exposed using a $\varphi$ rotation scan mode at constant times of 1.8 min per image. 48209 Reflections measured ($\theta_{max} = 30°$), 20707 unique ($R_{int} = 0.0506$) which were used in all calculations, 993 parameters in full matrix refinement. All three cyclohexyl groups bound to P2 are disordered (from difference electron density maps), and were refined using the PART option.[27] Final $R1 = 0.0616$, $wR2(F^2) = 0.1977$.

**[Re(NO)$_2$(PCy$_3$)$_2$(C$_6$H$_5$CHO)][BAr$^F_4$].** A slurry of [Re(NO)$_2$(PCy$_3$)$_2$][BAr$^F_4$] (50 mg, 0.0299 mmol) in $C_6H_6$ (1 mL) was treated with benzaldehyde (10 μL, 0.0984 mmol). In a few minutes the starting material dissolved and a brown solution was obtained. Pentane was layered over this solution and after 24 h red-brown crystals were collected, washed with pentane (2 × 10 mL) and dried *in vacuo* yielding 40 mg of **IV**$^+$[BAr$^F_4$]($C_6H_6$) (72.2%). IR($CD_2Cl_2$): $\nu_{CO,NO}$ 1704w, 1668s, 1651 (sh), 1617s, 1611s, 1593s and 1575m cm$^{-1}$. $^{31}$P-{$^1$H} NMR ($CD_2Cl_2$): $\delta$ 32.5 (s). $^1$H NMR ($CD_2Cl_2$): $\delta$ 9.92 (s, 1 H, $C_6H_5CHO$), 8.04–7.78 (m, 5 H, $C_6H_5$CHO), 7.73 (m, br, 8 H, BAr$^F_4$), 7.60 (m, br, 4 H, BAr$^F_4$) and 2.30–0.8 (m, 66 H, PCy$_3$). $^{13}$C-{$^1$H} NMR ($CD_2Cl_2$): $\delta$ 206.9 (s, br, $C_6H_5$*C*OH) [Calc. for $C_{75}H_{84}BF_{24}N_2O_3P_2Re$ (recrystallized in $CH_2Cl_2$–pentane): C, 50.71; H, 4.77; N, 1.58. Found: C, 50.67; H, 4.59; N, 1.58%].

*Crystal structure determination.* The compound crystallizes with three molecules $C_6H_6$ per asymmetric unit. Formula $C_{93}H_{102}BF_{24}N_2O_3P_2Re$, $M = 2010.79$, triclinic, space group $P\bar{1}$ (no. 2), $a = 13.892(3)$, $b = 18.768(3)$, $c = 19.569(3)$ Å, $\alpha = 97.76(2)$, $\beta = 107.96(2)$, $\gamma = 102.88(2)°$, $V = 4615.8(1.2)$ Å$^3$, $T = 153$ K, $Z = 2$, $\mu$(Mo-K$\alpha$) = 1.46 mm$^{-1}$, $\omega$ scan width 1.6°, variable scan speed 2–29° min$^{-1}$, 16060 reflections measured ($\theta_{max} = 25°$), 15223 unique ($R_{int} = 0.030$) which were used in all calculations, 1194 parameters in full matrix refinement, final $R1 = 0.0539$, $wR(F_{obs}) = 0.0385$. $\psi$-Scan reflections for absorption correction were measured, but did not lead to further improvement of the results. Therefore, the uncorrected data set was used in structure refinement. The F atoms for two of the trifluoromethyl groups had to be refined isotropically. One of the cyclohexyl groups appeared to be disorderd as well, and the four C atoms involved had to be split and refined with isotropic displacement parameters.

**[Re(NO)$_2$(P$^i$Pr$_3$)$_2$\{ONRe(NO)(P$^i$Pr$_3$)$_2$H\}]BAr$^F_4$].** A heterogeneous mixture of [Re(NO)$_2$(P$^i$Pr$_3$)$_2$H] (165 mg, 0.299 mmol) and [Ph$_3$C][BAr$^F_4$] (163 mg, 0.147 mmol) in $C_6H_6$ (15 mL) was stirred for 2 h. During this period an orange solid was formed. The solvent was removed *in vacuo* until *ca*. 3 mL of $C_6H_6$ were left and then pentane (15 mL) was added. The residue was washed with pentane (3 × 15 mL) and dried *in vacuo* to give 250 mg of **V**$^+$[BAr$^F_4$] (83.7%). Crystals for the X-ray diffraction study were grown by recrystallization of a diluted solution of the complex from $C_6H_6$–pentane. IR(Nujol): $\nu_{NO}$ 1659s, 1645m, 1627s and 1609s cm$^{-1}$. $^{31}$P-{$^1$H} NMR ($C_6D_5Cl$): $\delta$ 54.9 (s, br, 2P) and 43.3 (s, br, 2P). $^1$H NMR ($C_6D_5Cl$): $\delta$ 8.12 (m, br, 8H, BAr$^F_4$), 7.47 (m, br, 4 H, BAr$^F_4$), 3.39 (t, br, $J_{HP} = 46.8$ Hz, Re), 2.30 [m, br, 6 H, P(C*H*Me$_2$)$_3$], 2.05 [m, br, 6 H, P(C*H*Me$_2$)$_3$] and 0.95 [m, 72 H, P(CH*Me*$_2$)$_3$] (Calc. for $C_{68}H_{97}BF_{24}N_4O_4P_4Re_2$: C, 40.89; H, 4.89; N, 2.80. Found: C, 40.95; H, 4.84; N, 2.78%).

*Crystal structure determination*. The very small crystal size caused high residual electron density of 7.68 e Å$^{-3}$, 0.94 Å away from Re2. $C_{68}H_{97}BF_{24}N_4O_4P_4Re_2$, $M = 1997.61$, triclinic, space group $P\bar{1}$ (no. 2), $a = 14.256(2)$, $b = 16.859(2)$, $c = 17.771(2)$ Å, $\alpha = 97.22(1)$, $\beta = 93.87(1)$, $\gamma = 96.11(1)°$, $V = 4198.9(0.8)$ Å$^3$, $T = 183$ K, $Z = 2$, $\mu$(Mo-K$\alpha$) = 3.09 mm$^{-1}$, $\omega$ scan width 1.2°, variable scan speed 2–29° min$^{-1}$, 15369 reflections measured ($\theta_{max} = 25°$), 14579 unique ($R_{int} = 0.020$), 10254 reflections used in all calculations. Isopropyl groups are disordered; 962 parameters in full matrix refinement, final $R1 = 0.1104$, $wR(F_{obs}) = 0.081$. Owing to the small crystal dimensions, five C atoms of four isopropyl groups, as well as one C atom of the BAr$^F_4$ anion, had to be refined isotropically.

### Computational details

All calculations were based on the local density approximation (LDA) in the parameterization of Vosko *et al.*[32] with the addition of gradient corrections due to Becke[33] and Perdew[34] (BP86), which were included self-consistently (NL-SCF). The calculations utilized the Amsterdam Density Functional package ADF,[35] release 2.3. Use was made of the frozen core approximation, and the *n*s, *n*p, *n*d and ($n$ + 1)s shells of the transition metal were described by a triple ζ-STO basis augmented by one ($n$ + 1)p function (ADF database IV). The valence shells of the main group atoms were described by a double ζ-STO basis plus one polarization function (ADF database III). The numerical accuracy[35b,d] was set to 5.0, and final gradients were $2.0 \times 10^{-3}$ au Å$^{-1}$ and better. If not mentioned otherwise, calculations were performed under $C_{2v}$ or $C_s$ symmetry constraints. Relativistic effects were included using a quasi-relativistic approach.[36]

## Acknowledgements

This work was supported by the Swiss National Science Foundation (SNSF). Access to the computing facilities of the Rechenzentrum der Universität Zürich is gratefully acknowledged.

## References

1 G. B. Richter-Addo and P. Legdins, *Metal Nitrosyls*, Oxford University Press, New York, NY, 1992; M. Feelisch and J. S. Stammler (Editors), *Methods in Nitric Oxide Research*, Wiley, Chichester, 1996.
2 H. Berke and P. Burger, *Comments Inorg. Chem.*, 1994, **16**, 279.
3 A. A. H. van der Zeijden, T. Bürgi and H. Berke, *Inorg. Chim. Acta*, 1992, **201**, 131.
4 A. A. H. van der Zeijden, C. Sontag, H. W. Bosch, V. Shklover,

H. Berke, D. Nanz and W. von Philipsborn, *Helv. Chim. Acta*, 1991, **74**, 1194; A. A. H. van der Zeijden, V. Shklover and H. Berke, *Inorg. Chem.*, 1991, **23**, 4393; A. A. H. van der Zeijden, H. W. Bosch and H. Berke, *Organometallics*, 1992, **11**, 563; 2051.
5 H.-U. Hund, U. Ruppli and H. Berke, *Helv. Chim. Acta*, 1993, **76**, 963; H.-U. Hund, Ph.D. Thesis, Zürich, 1991.
6 S. Feracin, T. Bürgi, V. I. Bakhmutov, I. Eremenko, E. V. Voronstov, A. B. Vimentis and H. Berke, *Organometallics*, 1994, **13**, 4194; V. Bakhmutov, T. Bürgi, P. Burger, U. Ruppli and H. Berke, *Organometallics*, 1994, **13**, 4203; E. S. Shubina, N. V Belkova, A. N. Krylov, E. V. Vorontsov, L. M. Epstein, D. G. Gusev, M. Niedermann and H. Berke, *J. Am. Chem. Soc.*, 1996, **118**, 1105; N. V. Belkova, E. S. Shubina, A. V. Ionidis, L. M. Epstein, H. Jacobsen, A. Messmer and H. Berke, *Inorg. Chem.*, 1997, **36**, 1522.
7 D. Nietlispach, H. W. Bosch and H. Berke, *Chem. Ber.*, 1994, **127**, 2403.
8 D. G. Gusev, A. Llamazares, G. Artus, H. Jacobsen and H. Berke, *Organometallics*, 1999, **17**, 75.
9 T. Ziegler, *Chem. Rev.*, 1991, **91**, 651; J. Labanowski and J. Andzelm (Editors), *Density Functional Methods in Chemistry*, Springer, Heidelberg, 1991; T. Ziegler, *Can. J. Chem.*, 1995, **73**, 743; B. B. Laird, R. B. Ross and T. Ziegler, *ACS Symp. Ser.*, 1996, **629**.
10 (*a*) D. M. P. Mingos and J. A. Ibers, *Inorg. Chem.*, 1970, **9**, 1105; (*b*) A. P. Gaughan Junior, B. J. Corden, R. Eisenberg and J. A. Ibers, *Inorg. Chem.*, 1974, **13**, 786; (*c*) V. G. Albano, A. Araneo, P. L. Bellon, G. Ciani and M. Manassero, *J. Organomet. Chem.*, 1974, **67**, 413; (*d*) B. L. Haymore and J. A. Ibers, *Inorg. Chem.*, 1975, **14**, 2610; (*e*) J. A. Kaduk and J. A. Ibers, *Inorg. Chem.*, 1975, **14**, 3070; (*f*) S. Bhaduri and G. M. Sheldrick, *Acta Crystallogr.*, *Sect. B*, 1975, **31**, 897; (*g*) B. E. Reichert, *Acta Crystallogr.*, *Sect. B*, 1976, **32**, 1934; (*h*) J. A. Kaduk and J. A. Ibers, *Inorg. Chem.*, 1977, **16**, 3283; (*i*) A. M. M. Lanfredi, A. Tiripicchio and M. Tiripicchio Camellini, *Acta Crystallogr.*, *Sect. C*, 1983, **39**, 1633; (*j*) G. Le Borgne, L. Mordenti, J. G. Riess and J.-L. Roustan, *New J. Chem.*, 1986, **10**, 97; (*k*) H. Li Kam Wah, M. Postel and M. Pierrot, *Inorg. Chim. Acta*, 1989, **165**, 215; (*l*) V. Munyejabo, J.-P. Damiano, M. Postel, C. Bensimon and J.-L. Roustan, *J. Organomet. Chem.*, 1995, **491**, 61; (*m*) F. L. Atkinson, H. E. Blackwell, N. C. Brown, N. G. Connelly, J. G. Crossley, A. G. Orpen, A. L. Rieger and P. H. Rieger, *J. Chem. Soc.*, *Dalton Trans.*, 1996, 3491.
11 R. H. Summerville and R. Hoffmann, *J. Am. Chem. Soc.*, 1976, **98**, 7240.
12 S. C. Haefner, K. R. Dunbar and C. Bender, *J. Am. Chem. Soc.*, 1991, **113**, 9540.
13 M. Ogasawara, S. A. Macgregor, W. E. Streib, K. Folting, O. Eisenstein and K. G. Caulton, *J. Am. Chem. Soc.*, (*a*) 1995, **117**, 8869; (*b*) 1996, **118**, 10189.
14 T. A. Albright, J. K. Burdett and M.-H. Whangbo, *Orbital Interactions in Chemistry*, Wiley, New York, NY, 1985, (*a*) ch. 19.1; (*b*) ch. 15.4.
15 M. Elian and R. Hoffmann, *Inorg. Chem.*, 1975, **14**, 1058.
16 K.-P. Huber and G. Herzberg, *Molecular Spectra and Molecular Structure*, Van Nostrand Reinhold, New York, NY, 1979, vol. IV.
17 R. Hoffmann, L. M. Chen, M. Ellian, A. R. Rossi and D. M. P. Mingos, *Inorg. Chem.*, 1974, **13**, 2666; A. R. Rossi and R. Hoffmann, *Inorg. Chem.*, 1975, **14**, 365; R. Hoffmann, J. M. Howell and A. R. Rossi, *J. Am. Chem. Soc.*, 1976, **98**, 2484.
18 (*a*) E. L. Muetterties, *Tetrahedron*, 1974, **30**, 1595; (*b*) E. L. Muetterties and L. J. Guggenberger, *J. Am. Chem. Soc.*, 1974, **96**, 1748.
19 D. H. Mordaunt, H. Flöthmann, M. Stumpf, H.-M. Keller, C. Beck, R. Schinke and K. Yamashita, *J. Chem. Phys.*, 1997, **107**, 6603.
20 T. Ziegler and A. Rauk, *Theor. Chim. Acta*, 1977, **46**, 1; *Inorg. Chem.*, 1979, **18**, 1558; T. Ziegler, *NATO ASI*, *Ser. C*, 1992, **378**, 367; F. M. Bickelhaupt, N. M. M. Nibbering, E. M. van Wezenbeek and E. J. Baerends, *J. Phys. Chem.*, 1992, **96**, 4864.
21 H. Jacobsen and T. Ziegler *J. Am. Chem. Soc.*, 1994, **116**, 3667.
22 A. Llamazares, H. W. Schmalle and H. Berke, in preparation.
23 IPDS Software, Stoe and Gie, Darmstadt, Germany, 1997.
24 SHELXTL PLUS, Siemens Analytical X-Ray Instruments, Madison, WI, 1994.
25 P. Coppens, L. Leiserowitz and D. Rabinovich, *Acta Crystallogr.*, 1965, **18**, 1035.
26 G. M. Sheldrick, *Acta Crystallogr.*, *Sect. A*, 1990, **46**, 467.
27 A. Altomare, G. Cascarano, C. Giacovazzo, A. Guagliardi, M. C. Burla, G. Polidori and M. Camalli, SIR 92, University of Bari, 1992.
28 G. M. Sheldrick, SHELXL 97, University of Göttingen, 1997.
29 D. J. Watkin, C. K. Prout, J. R. Carruthers and P. W. Bettridge, CRYSTALS, Issue 10, Chemical Crystallography Library, University of Oxford, Oxford, 1996.
30 J. R. Carruthers and D. J. Watkin, *Acta Crystallogr.*, *Sect. A*, 1979, **35**, 698.
31 A. L. Spek, *Acta Crystallogr.*, *Sect. A*, 1990, **46**, C34.
32 S. J. Vosko, M. Wilk and M. Nussair, *Can. J. Phys.*, 1980, **58**, 1200.
33 A. D. Becke, *Phys. Rev. A*, 1988, **38**, 3098.
34 J. P. Perdew, *Phys. Rev. B*, 1986, **33**, 8822.
35 (*a*) E. J. Baerends, D. E. Ellis and P. E. Ros, *Chem. Phys.*, 1973, **2**, 41; (*b*) G. te Velde and E. J. Baerends, *J. Comput. Phys.*, 1992, **99**, 84; (*c*) C. Fonseca Guerra, O. Visser, J. G. Snijders, G. te Velde and E. J. Baerends, In *Methods and Techniques in Computational Chemistry: METECC-95*, eds. E. Clementi and G. Corongiu, STEF, Cagliari, 1995, p. 305; (*d*) G. te Velde, *ADF 2.1 User's Guide*, Vrije Universiteit, Amsterdam, 1996.
36 T. Ziegler, V. Tschinke, E. J. Baerends, J. G. Snijders and W. Ravenek, *J. Phys. Chem.*, 1989, **93**, 3050; G. Schreckenbach, J. Li and T. Ziegler, *Int. J. Quantum. Chem.*, 1995, **56**, 477.

*Paper 9/01384I*